ELSEVIER

Remote Sensing of Environment

www.elsevier.com/locate/rse

Characterization of Forests in Western Sayani Mountains, Siberia from SIR-C SAR Data

K. J. Ranson, G. Sun,† V. I. Kharuk‡ and K. Kovacs§*

This paper examines the use of space-borne radar data to map forest types and logging in the mountainous Western Sayani area in central Siberia. L- and C- band HH-, HV-, and VV-polarized images from the Shuttle Imaging Radar–C instrument were used in the study. Techniques to reduce topographic effects in the radar images were investigated. These included radiometric correction using illumination angle inferred from a digital elevation model and reducing apparent effects of topography through band ratios. Forest classification was performed after terrain correction utilizing typical supervised techniques and principal component analyses. An ancillary data set of local elevations was also used to improve the forest classification. Map accuracy for each technique was estimated for training sites based on Russian forestry maps, satellite imagery, and field measurements. The results indicate that it is necessary to correct for topography when attempting to classify forests in mountainous terrain. Radiometric correction based on a digital elevation model improved classification results but required reducing the synthetic aperture radar resolution to match the digital elevation model. Using ratios of synthetic aperture radar channels that include cross-polarization improved classification and had the advantages of eliminating the need for a digital elevation model and preserving the full resolution of the synthetic aperture radar data.

INTRODUCTION

The usefulness of synthetic aperture radar (SAR) for mapping forests has been demonstrated by several authors using different remote sensing systems and over various forest types (e.g., Rignot et al.,, 1994; Ranson et al., 1995; Dobson et al., 1996; Ranson and Sun, 1997a, 1997b; Saatchi and Rignot, 1997; Pierce et al., 1998). These studies, however, were all conducted in areas with low topographic relief. Since significant amounts of the world's forests grow in mountainous areas, techniques to effectively utilize SAR are needed. High-resolution optical remote sensing data such as SPOT and Landsat have been used to map mountainous terrain. These techniques included normalization with a digital elevation model (DEM) (e.g., Franklin, 1991; Colby and Keating, 1998, Gu et al., 1999), band ratios (e.g., Colby, 1991), radiation scattering models (e.g., Franklin, 1991; Colby and Keating, 1998), and empirical models (e.g., Smith et al., 1980; Ekstrand, 1996).

Topography greatly influences the radar backscatter through local incidence angle, shadowing, and layover effects (Leberl, 1990). The terrain effects on the radar signature impose severe constraints on the landscape mapping from radar data. However, few researchers have reported on techniques to address this problem. Kellendorfer et al. (1998) used a DEM for radiometric correction of radar backscatter due to differences in radar illumination areas. Shi and Dozier (1997) showed that correction of an SAR antenna pattern was possible using a DEM. Goering et al. (1995) used a DEM and empirical radar backscatter models to reduce terrain effects from ERS-1 SAR images. These and other researchers (e.g., Goyal et al., 1998) have found that the small-scale topographic features resolved by SAR could not be resolved by a DEM in rugged terrain. Periodic artifacts due to the terrain model generation methodology were observed in the derived variables (e.g., slopes). Other methods such as image ratios were used to reduce the effects of radar incidence angle caused by topography (Ranson and Sun, 1994; Shi and Dozier, 1997; Wever and Bodech-

* NASA's Goddard Space Flight Center, Code 923, Greenbelt, MD
† Department of Geography, University of Maryland, College Park, USA
‡ V. N. Sukachev Institute of Forest, Academgorodok, Krasnoyarsk, Russia
§ Science Systems and Applications, Inc., Lanham, MD, USA
Address correspondence to K. J. Ranson, NASA's Goddard Space Flight Center, Code 923, Greenbelt, MD 20771, USA. E-mail: jon@taiga.gsfc.nasa.gov
Received 25 February 2000; revised 21 July 2000.

655 Avenue of the Americas, New York, NY 10010

0034-4257/00/$–see front matter
PII S0034-4257(00)00166-8

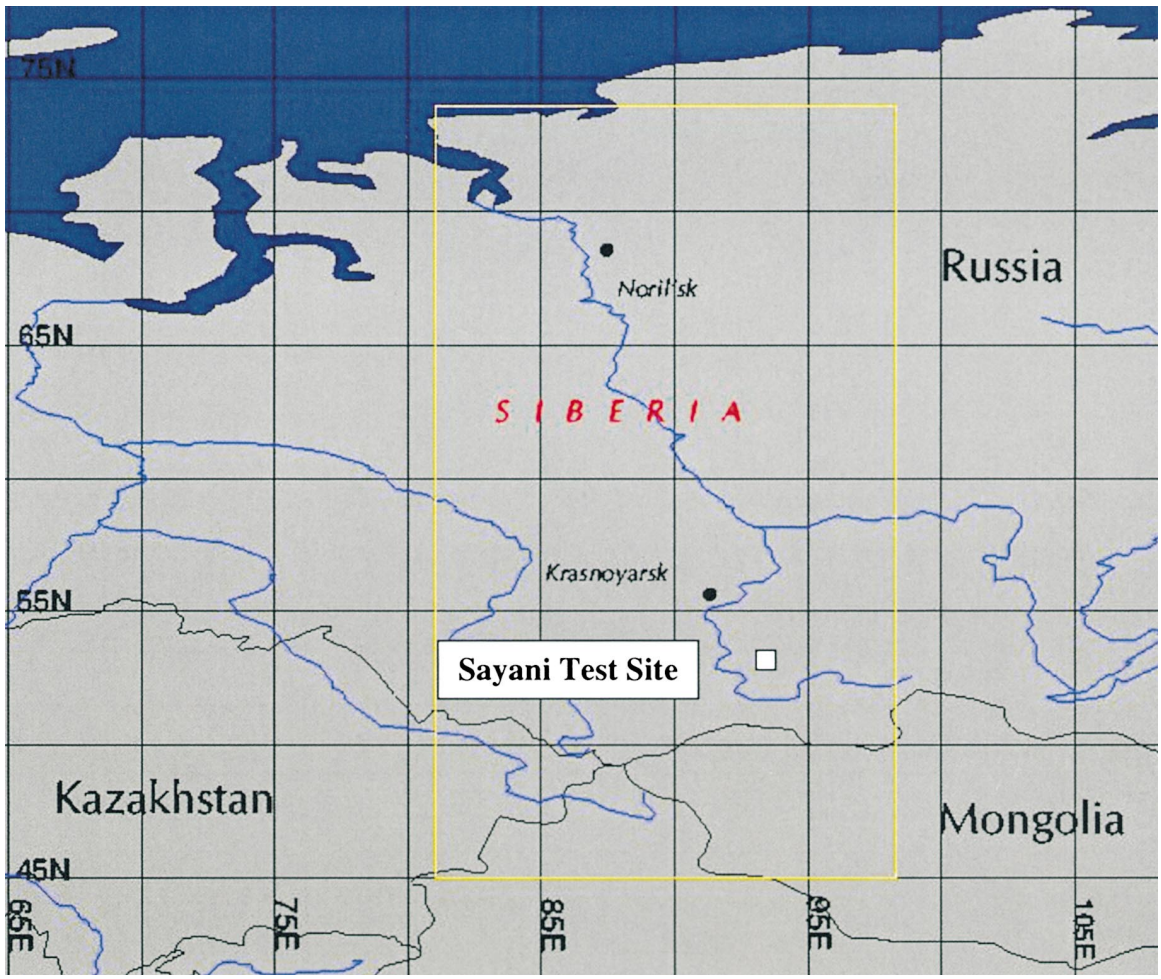

Figure 1. Map of test area location in central Siberia, Russia.

tel, 1998). The angular dependencies of radar backscattering from sloped surfaces are similar for different wavelengths and polarizations (Ulaby et al., 1986); thus, a ratio of two channels will reduce the effects of slope. Wever and Bodechtel (1998) discussed the use of a ratio of SIR-C/XSAR L-band HV and X-band VV backscatter for radiometric rectification in mountainous terrain.

Within the Siberian region, where our study is located, mountainous areas comprise about 50% of the forested terrain. Generally, high resolution optical data have not been used to map and monitor this area, because of the frequent cloud cover, low sun angle, and lack of local ground receiving stations. The latter problem has improved somewhat since the April 15, 1999 launch of Landsat 7.

Table 1. Forestry Map Classes and Reduced Set for SAR Analysis, with Number of Training and Testing Pixels Also Shown

Map Class	*Description*	*SAR Class (Code)*	*Training Pixels*	*Testing Pixels*
Clearcut	Recently cleared areas	Clearcut (CC)	431	279
Wetlands	Vegetation in perpetually wet areas	Wetlands (WET)	1,070	337
Snow	Snow-covered areas	Snow (SNW)	451	493
Old aspen	Mature stands of aspen	Old deciduous (OD)	1,192	256
Old birch	Mature stands of birch			
Young aspen	Immature stands of aspen	Young deciduous (YD)	845	310
Young birch	Immature stands of birch			
Old cedar	Mature stands of Siberian pine	Old conifer (OC)	625	922
Old fir	Mature stands of Siberian fir			
Young cedar	Immature stands of Siberian cedar	Young conifer (YC)	451	493
Young fir	Immature stands of Siberian fir			

Radar data with its ability to penetrate clouds promises to be useful for monitoring forests and other landscapes in this area if terrain effects can be reduced. In this study, the use of DEM correction and image ratio techniques to reduce the effects of terrain on forest classification are presented and discussed.

STUDY AREA

The Western Sayani test area covers a 50×25 km area with center coordinates of 53° 4.2′ N latitude and 93° 14.3′ E longitude (Fig. 1). The area is part of the dark-coniferous taiga forests that grow in mountainous regions (300–1,800 m above mean sea level). The forests of this area include cedar (*Pinus siberica*), fir (*Abies sibirica*), aspen (*Populus tremula*), and birch (*Betula verrocosa*, B. *pubescens*, *Betula* spp.). The climate is continental with wet summers and cold dry winters. Temperature and precipitation are strongly controlled by elevation. Annual precipitation varies from 560 mm in the lower regions to 1,300 mm at higher elevations. Tree line occurs at about 1,800 m. The study area includes the Ermakovsky Permanent Study Area established in 1959, which is used for forest and ecological research by the Sukachev Institute of the Siberian Branch of the Russian Academy of Sciences.

A Russian forest inventory map (1:50,000) compiled from aerial photographs and field checks between 1993 and 1995 was used as ground truth information. The map is typical of forest inventory maps with forest units related to economic value of the stands. The forest map also included an intermediate age class for some of the forest categories and several nonforest classes. Because of the paucity of these sites and the related difficulties encountered in finding adequate training areas, the intermediate age classes were not included in this study. A reduced set of classes was developed by combining deciduous or conifer species types, however, and old and young designations were retained. In addition to forest classes from the inventory map, other classes were added to represent logging as clear cuts, as well as wetlands and snow. Snow class was included since field measurements during the April 1994 SIR-C mission indicated significant snow cover at higher elevations (Kharuk et al., 1999). The resulting seven cover classes are listed in Table 1.

Training areas for each of the original map classes were identified on the forestry maps and located on the SAR images. A set of test areas were found (multiple sites for each class) with the aid of the forest map and available high resolution satellite imagery. Images for a July 1999 Landsat 7 ETM+, August 1991 SPOT HRV, and a 1983 Russian Resours F image were available. Approximately one-third of the image pixels from these sites were set aside as testing sets. Table 1 lists the number of pixels used for training and testing purposes.

SIR-C/XSAR

The satellite data used in this study was SAR data from the Shuttle Imaging Radar/X-band SAR (SIR-C/XSAR) mission. SIR-C/X-SAR was part of a series of space-borne imaging radar missions that began with the June 1978 launch of Seasat SAR and continued with the November 1981 SIR-A and October 1984 SIR-B missions. The SIR-C/X-SAR missions were successfully conducted during April 9–19, 1994 and September 30–October 10, 1994 and demonstrated the design and capabilities of a space-borne multifrequency polarimetric SAR (Stofan et al., 1995). The instrument had quad-polarized (HH, HV, VV, HV) L-band (wavelength=23 cm) and C-band (5.6 cm) radar and VV-polarized X-band (3 cm) radar channels. The SIR-C/X-SAR design included bandwidths of 10, 20, and 40 MHz. The instrument augmented the present and still current configurations of orbiting radar systems such as the C-band VV-polarized ERS-1 and C-band HH-polarized RADARSAT and the (now defunct) L-band HH-polarized JERS-1 systems. The mission was a cooperative experiment between NASA, the German Space Agency, and the Italian Space Agency. SIR-C/X-SAR was launched on space shuttle Endeavor and acquired multiple data takes covering over 6% of the Earth's surface including a variety of land, ocean, and ice targets. Currently SIR-C data are available through the EROS Data Center in Sioux Falls, South Dakota, USA.

METHODS

This work employed approaches for reducing topographic effects on forest classification and utilizing ancillary information including topography to produce the best classification possible for our mountainous test site. This section discusses radiometric correction after computing local incidence angle from a DEM and topographic effect reduction using SAR channel ratios. The best method was selected and used with the ancillary data to further improve the classification.

Radiometric Correction with a DEM

For this study area, the DEM available for use was Digital Terrain Elevation Data (DTED) Level 1 (3 arc second pixel spacing) from the U.S. Department of Defense. The DEM offers a pixel spacing of roughly 90×90 M at the Earth's equator and a nominal accuracy of ±30 m. The pixel spacing at the latitude of our study area was about

Table 2. Radar Parameters used for Image Simulation from DEM

Output pixel size	26.649 m×34.555 m
Platform altitude	223.4574 km
Platform heading angle	71.1443329
Minimum look angle	46.08°
Location of first pixel	53.1489372° N 92.7996979° E

Figure 2. LHV image of the Sayani test site showing mountains on the right side.

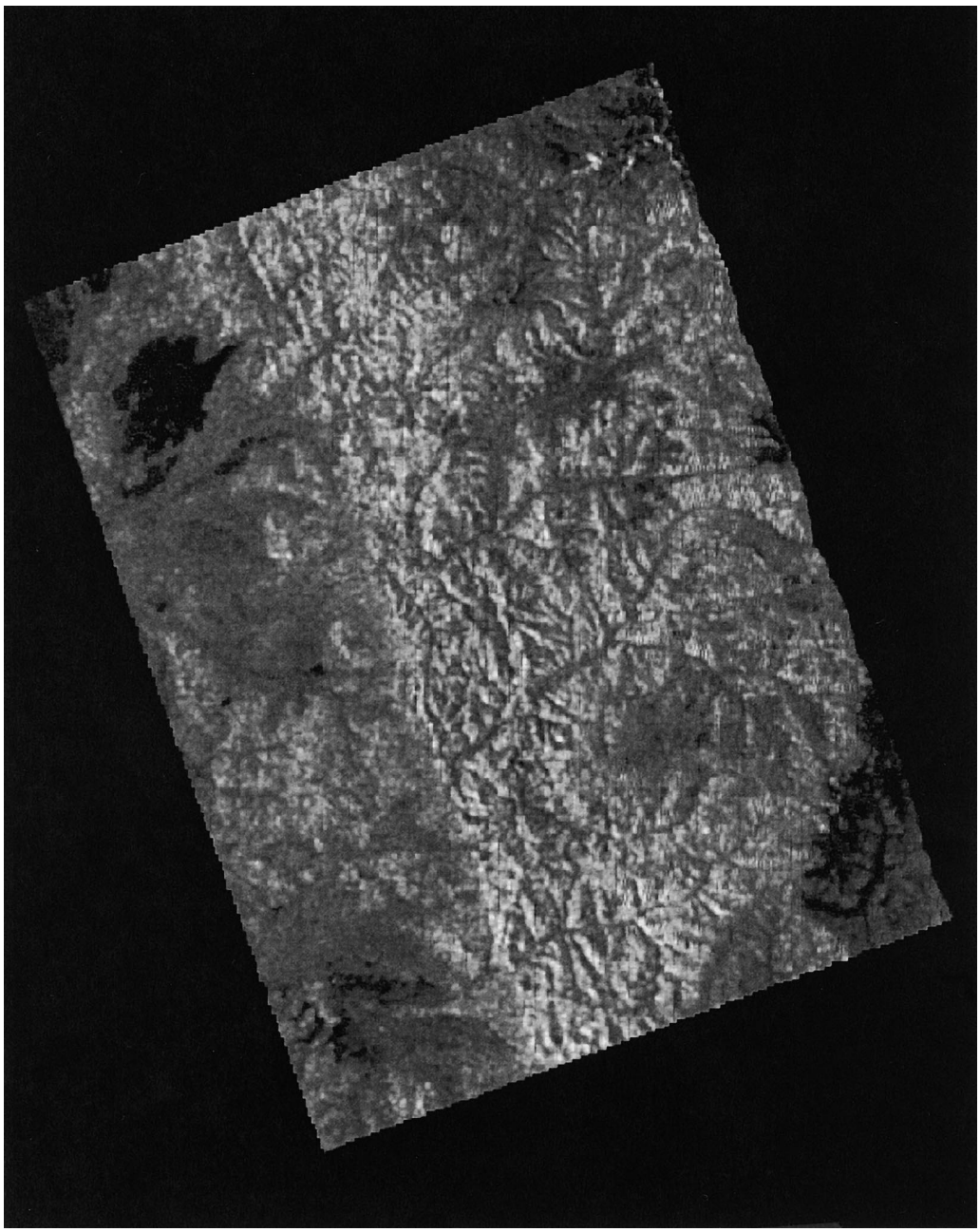

Figure 3. LHV image that was terrain-corrected using a DEM.

50×90 m. The DEM was resampled to 50×50 m pixels. The use of low resolution DEM for geocoding and radiometric correction of the higher resolution radar images (∼30 m) was unsatisfactory because of the difficulty in matching control points. Therefore, the resolution of the radar images was reduced to the resolution of DEM. To facilitate identification of control points on both SAR and DEM images, a radar image was simulated based on the DEM and the mission, sensor, and image parameters provided by Jet Propulsion Laboratory (JPL) (Table 2). Ground control points were selected from both SIR-C and simulated SAR images and were used to orthorectify and geocode the radar images to the DEM. Slope and aspect were generated from the DEM and were used to calculate the local incidence angle for every pixel of the image.

The SIR-C image data used in this study were acquired on April 16, 1994 with an image center incidence angle of 46.4° and bandwidth of 10 MHz. The SAR channels used were L-band and C-band with HH, HV, and VV polarizations. The L- and C-band images (LHH, LHV, HVV, CHH, CHV, CVV) were processed with six looks in azimuth and converted from slant to ground range resulting in a pixel size of ∼30 m. To reduce image speckle, the images were filtered using Lee filter with a 5×5 pixel window as de-

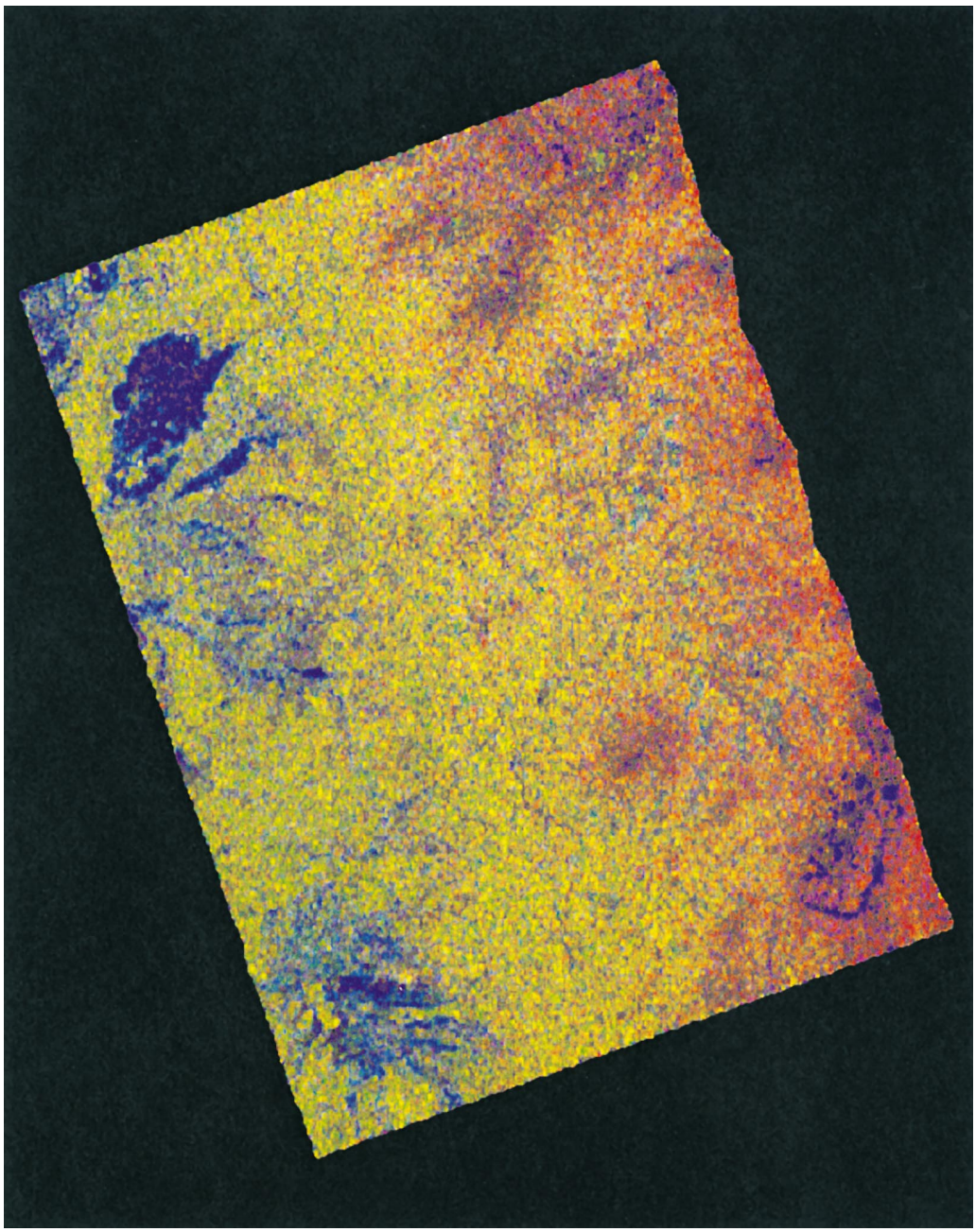

Figure 4. Composite image of Sayani test site using ratios of SIR-C Channels: LHH/LVV=red, LHV/CVV=green, and LHH/LHV=blue.

scribed in PCI (1998). Figure 2 is the LHV image of the test site showing obvious topography effects. The resolution of the SIR-C image data was reduced to about 50 m by spatial averaging and was registered to the DEM-simulated image. Registration was accomplished with 21 control points and a first-order nearest neighbor resampling routine of PCI (1998).

Slope and aspect were generated from the DEM and were used to calculate the local incidence angle for every pixel of the image as shown in Eq. (1):

$$\cos(i)=\cos(a_s)\cdot\cos(a)+\sin(a_s)\cdot\sin(a)\cdot\cos(\boldsymbol{a}-\boldsymbol{a}_s) \qquad (1)$$

Table 3. Eigenvalues and Percent Variation Accounted for the First Six Principal Components

PC	*Eigenvalue*	*Variation %*
1	5.441	64.1
2	1.9412	22.9
3	0.4500	5.30
4	0.4011	4.73
5	0.1142	1.35
6	0.0766	0.90

Table 4. First Six Principal Component Coefficients for 15 SIR-C Channnel Ratios

	Principal Component					
Ratio	*1*	*2*	*3*	*4*	*5*	*6*
LHV/CVV	−0.0003	0.2322	0.0641	0.0103	−0.0904	−0.0798
LHH/LVV	−0.0139	−0.0122	0.3520	−0.2133	−0.0728	0.0635
CHH/CVV	0.0469	0.0389	−0.0188	0.0185	0.3179	0.4233
LHH/CHV	0.5339	0.4993	0.3982	−0.3105	−0.1236	−0.0919
LHV/CHH	−0.0164	0.0585	−0.0966	−0.0571	−0.3614	0.2323
LHV/CHV	−0.0003	0.2322	0.0641	0.0103	−0.0904	−0.0798
LHH/LHV	0.6726	−0.6779	−0.0460	−0.1518	−0.0576	−0.0247
LHH/CHH	0.0583	0.1235	−0.0385	−0.2759	−0.0156	−0.0802
LHH/CVV	0.1307	0.1664	−0.0740	−0.2877	0.4226	0.4434
LHV/LVV	−0.0260	0.0265	0.0673	−0.0323	−0.0508	−0.0020
LVV/CHH	0.0391	0.0929	−0.3942	−0.0977	−0.6534	0.4494
LVV/CHV	0.4182	0.3341	−0.5207	0.3870	0.0896	−0.3249
LVV/CVV	0.0998	0.1173	−0.2784	−0.0513	0.3188	0.2579
CHH/CHV	0.2287	0.0228	0.4247	0.7125	−0.0714	0.3937
CHV/CVV	−0.0029	0.0068	−0.0404	−0.0414	0.0709	0.0947

where i=local incidence angle, a_s=local slope angle, a=incidence angle of SAR beam at the center of image, $\boldsymbol{\alpha}_s$=aspect of slope (north=0°), and $\boldsymbol{\alpha}$=azimuth angle of SAR beam.

Radiometric distortion due to the illumination area was corrected using this angle by the equation used by Kellndorfer et al.(1998) [see Eq. (2)]:

$$I_{corr} = \mathrm{DN} \cdot [\sin(i)/\sin(i_{ref})] \quad (2)$$

where I_{corr}=radar signal intensity corrected for local incidence angle, i=local incidence angle at each pixel, and i_{ref}=the radar incidence angle at the center of the image.

Kellendorfer et al. (1998) have found that this correction was adequate for land cover classification purposes. Figure 3 is the LHV image corrected in this manner. Because of the low resolution of the available DEM data, the results obtained do not appear to be very satisfactory since there are residual topographic effects in the image. Because the best available DEM data was used and there was reduction in the overall topographic features, this approach was applied to all six SAR channels to produce radiometrically "corrected" images. In the future, new data sets such as that from the Shuttle Radar Topography Mission (SRTM) should improve the DEM quality.

The initial classification approach used the six uncorrected SIR-C channels in a supervised maximum likelihood classifier available with the PCI analysis system. The second classification used a similar method with the six channels of SAR data radiometrically corrected using Eqs. (1) and (2).

Channel Ratios

A third method of classification using selected band ratios was also used to attempt to reduce topographic effects. As discussed above, band ratios can be used since backscatter dependence on slope is similar for different frequencies and polarizations (Ulaby et al., 1986). Band ratios were calculated from intensity (power) units to produce six nonredundant single band combinations (e.g., LHH/LVV) and nine nonredundant two-band combinations (e.g., LHH/CHV). Figure 4 presents a three-band image (LHV/LVV: red, LHV/CVV: green, and LHH/LHV: blue). It is obvious that the ratios reduce apparent topography while retaining some forest cover information as seen in the image.

A principal component analysis (PCA) approach was used to help separate useful information from noise and to reduce the dimensionality of data. Table 3 lists the first six principal components (PCs) and the percent of the variation accounted for. Table 4 lists the first six PCs (eigen-

Table 5. Classification Results Using Six Uncorrected SIR-C Channels

	YD	*OD*	*YC*	*OC*	*CLC*	*WTL*	*SNW*
YD	61.07	14.29	13.26	10.91	0.48	0.00	0.00
OD	15.86	69.25	6.04	4.25	4.18	0.43	0.00
YC	7.90	12.10	61.66	9.63	8.65	0.00	0.00
OC	6.28	9.45	14.91	68.84	0.64	0.00	0.00
CLC	0.00	5.60	5.80	2.80	83.10	2.60	0.20
WTL	0.80	3.10	0.70	0.40	7.90	86.40	0.70
SNW	0.20	2.40	0.00	4.20	0.70	4.70	87.80

Table 6. Classification Results for Six Radiometrically Corrected SIR-C Channels

	YD	*OD*	*YC*	*OC*	*CLC*	*WTL*	*SNW*
YD	66.62	17.36	9.82	6.14	0.00	0.00	0.00
OD	15.96	75.65	6.23	1.69	0.44	0.19	0.00
YC	7.75	4.42	79.40	7.56	0.87	0.00	0.00
OC	3.82	11.52	21.09	63.19	0.30	0.00	0.00
CLC	0.00	7.20	3.00	3.20	85.60	0.90	0.00
WTL	1.10	2.80	0.80	0.70	3.40	90.80	0.40
SNW	0.20	0.90	0.00	4.40	0.00	1.30	93.10

Table 7. Classification Results for Four Principal Components from Band Ratios

	YD	*OD*	*YC*	*OC*	*CLC*	*WTL*	*SNW*
YD	67.95	21.63	4.24	6.13	0.00	0.00	0.00
OD	14.02	83.45	0.18	0.75	0.84	0.77	0.00
YC	4.13	0.00	74.67	19.38	1.83	0.00	0.00
OC	6.55	2.72	7.18	82.39	1.12	0.00	0.00
CLC	0.00	0.20	0.00	0.50	99.30	0.00	0.00
WTL	0.00	6.00	0.00	0.00	0.10	92.90	1.00
SNW	0.00	0.00	0.00	0.00	0.00	2.20	97.80

vectors) with the coefficients for the 15 ratio elements. Class separability measures for each PC were calculated from class means and covariance matrices as Bhattacharrya Distances (BD) with the SIGSEP routine as described by PCI (1998).

The first principal component has strong contributions from LHH/CHV, LHH/LHV, LVV/CHV, CHH/CHV, and LHH/CVV, all with positive coefficients. The remaining ratio variables for PC1 had positive or negative coefficients that were very close to zero. The first PC showed very good separability (BD>1.9) for clear cuts with forest classes, good separability (1.0>BD>1.9) for forest classes and snow, and good to very good separability of deciduous and conifer classes.

The second PC has greatest contribution from LHH/CHV, LHH/LHV, and, to a lesser extent, LHH/CHV, with the greatest contribution from copolarization to cross-polarization ratios. The negative coefficient of LHH/LHV suggests a ratio of CHV to LHV that is sensitive to forest biomass levels (e.g., Ranson and Sun, 1997a). The second PC had very good separability (BD>1.9) between most forest classes and nonforest classes, especially snow.

PC3 is a combination of many ratios that can be combined to approximate CHH/LVV and LHH/LVV. Such copolarization ratios may be more sensitive to forest structure. This is indicated by good to very good BD separability between conifer and deciduous classes.

The most important contributor to PC4 is CHH/CHV. This may also show the difference between low-vegetated area and bare surfaces similar to the first PC. However, for this PC the BD analysis showed poor separability between all classes.

Table 8. Classification Results for Training Areas Using Six Principal Components

	YD	*OD*	*YC*	*OC*	*CLC*	*WTL*	*SNW*
YD	73.03	21.77	3.55	1.64	0.00	0.00	0.00
OD	11.59	86.62	0.07	0.50	0.19	1.09	0.00
YC	3.57	0.56	82.61	12.78	0.40	0.00	0.00
OC	4.50	1.60	8.47	83.36	2.07	0.00	0.00
CLC	0.00	0.00	0.00	0.00	100.0	0.00	0.00
WTL	0.00	3.20	0.00	0.00	0.00	96.70	0.10
SNW	0.00	0.00	0.00	0.00	0.00	0.20	99.80

Table 9. Classification Results for Testing Areas Using Six Principal Components

	YD	*OD*	*YC*	*OC*	*CLC*	*WTL*	*SNW*
YD	65.79	30.99	1.95	1.32	0.00	0.00	0.00
OD	15.20	69.85	2.64	4.63	1.64	5.95	0.00
YC	11.29	6.02	50.80	27.41	4.42	0.00	0.00
OC	1.72	4.26	20.30	56.37	6.00	1.32	10.03
CLC	0.00	1.10	.60	2.20	93.20	0.00	0.00
WTL	0.00	5.90	0.00	0.00	0.90	93.20	0.00
SNW	0.00	9.70	0.00	0.00	1.80	11.00	77.50

The fifth and sixth PCs have greatest contribution from copolarization ratios (e.g., LVV/CHH, LHH/CVV, and CHH/CVV) with inclusion LHV/CHH for the fifth PC and CHH/CHV for the sixth PC. BD analysis showed good to very good separability between deciduous classes and clear cuts and deciduous classes and conifer classes for both PCs.

The first four principal components of the ratio images, accounting for over 97% of the variation in the transformed data set (Table 3), were used in a supervised maximum likelihood classification (PCI, 1998). The fifth and sixth PCs were added so that the same number of features were used as the first two classifications. This makes comparison of the classification results more straightforward since the number of features has an impact on the classification accuracy.

Classification maps were generated for the uncorrected data, radiometrically corrected data, and the principal components of ratio data, both four PCs and six PCs. A comparison of the results was made by examining the classification of the training and test area data sets.

RESULTS AND DISCUSSION

Uncorrected Data

A baseline classification that disregarded the effects of topography when classifying mountainous landscapes was performed with SIR-C data resampled to 50 m pixels (Table 5). Average classification accuracy was 71% with forest classes producing the lowest accuracies (<70% of forest class training set pixels correctly classified). Of course, results with uncorrected data may be improved by selecting classes based on topography (e.g., front- or rear-facing slopes), but this was not done to maintain consistency across the classifications of SIR-C data. Nonforest classification accuracies were generally good (>80%). Overall classification accuracy of the testing data was only 41% correct with a kappa of 0.31. Forest pixels were correctly classified were only 40% of the time.

Radiometrically Corrected Data

Table 6 lists the training set classification results obtained using the radiometric correction procedure described in the Methods section. The correction algorithm was dependent on the quality of the DEM and accuracy of image

Table 10. Summary Comparison of Classification Performance Statistics for Classification Methods

Classification Scheme	*Percentage Correct*		*Kappa*	
	Training Data	*Testing Data*	*Training Data*	*Testing Data*
Six SAR channels, uncorrected	71.6	41.9	0.66	0.31
Six SAR channels, radiometrically corrected	76.7	45.5	0.72	0.36
Four PCs from ratioed channels	83.3	69.3	0.80	0.63
Six PCs from ratioed channels	87.4	71.6	0.85	0.66
Six PCs from ratioed channels with elevational rules	87.9	71.6	0.85	0.65

registration. The results improved by about 5% for both training areas and test areas. Average accuracy improved to over 76% with the accuracy of nonforest classes better than 85%. Forest type classification also improved, but there are still errors in discriminating between forest type and age classes. For example, over 17% of the young deciduous class was mislabeled as old deciduous (OD), and over 21% of old conifer (OC) was mislabeled as young conifer (YC). The kappa statistic improved slightly to 0.36, which is still very poor.

Channel Ratios

Because of the problems inherent in trying to register SAR data to digital elevation model data, we decided to use SAR channel ratios to avoid the geometric and radiometric correction steps in the classification. SAR channel ratios have been shown in the past to reduce topographic effects (e.g., Ranson and Sun, 1997b; Wever and Bodechtel 1998) Therefore we used the available ratios developed from the six channels of SIR-C data as discussed above. The first four principal components were selected for the classification as discussed in the Methods section. The results are shown in Table 7 with average accuracy modestly better than the radiometrically corrected data at 83%. Testing data improved to 69% overall correct. Forest type classification improved for training and testing areas compared to the previous example, especially for the old conifer and deciduous classes. Nonforest class accuracies were all above 90% for the training set data. For test areas, wetland and clear cut accuracies were above 89%, but snow classification accuracy was only 77% with most confusion with wetland. Kappas for training and testing data were 0.80 and 0.63, respectively.

An additional classification was performed with the inclusion of the fifth and sixth principal components. The rationale for adding these components was to increase the number of channels to six so that the classifications with the six SIR-C channels could be easily compared. In addition, it is assumed that the sensitivity to forest structure can be enhanced by adding PCs with copolarized channel ratios (Table 4). Studies (e.g., Wu and Sader, 1987; Paris and Woodruff, 1991) have demonstrated that copolarized ratios such as LHH/LVV are useful for identifying canopy structure differences (e.g., bole and branch arrangements). This ratio is also sensitive to the presence of trunk-ground interactions, because this interaction produces a larger HH/VV ratio (Durden et al., 1991; Sun at al., 1991). The classification results are listed in Table 8. Average accuracy improved slightly to about 83% with excellent results for nonforest classes (>95%). Forest type discrimination improved with old deciduous accuracy increasing to nearly 87%. Young deciduous classification performance improved by 5%, but still was confused with other forest classes 22% of the time. Young and old conifer classification improved over the four PC analyses. Again these two classes were mostly misclassified with each other or to a lesser extent with young deciduous.

Classification results from the test areas are also shown in Table 9. The test area results showed similar trends to training data sets but with 10–20% lower accuracy. While individual young and old forest class accuracies were not very good, it appears that combining old and young classes would result in acceptable performance for deciduous (i.e., 90% for deciduous and 77% for conifer). The lower classification results for conifer classes may be due in part to the practice of foresters of identifying an entire stand of trees as old conifer even if there are only a few trees of this type present.

Table 11. Percent of Classified Images Occupied by Land Cover Classes

Name	*Percent Image*				
	Uncorrected	*Radiometrically Corrected*	*4 PCs*	*6 PCs*	*6 PCs with Elevation*
CLC	4.6	1.1	4.2	2.5	2.5
YD	15.8	16.3	10.3	9.9	9.7
OD	26.6	25.1	26.7	26.5	21.9
WTL	2.0	1.7	3.9	5.2	5.2
OC	28.9	32.0	18.9	18.5	23.0
YC	17.0	19.7	22.9	25.7	26.0
SNW	5.1	4.1	13.1	11.7	11.7

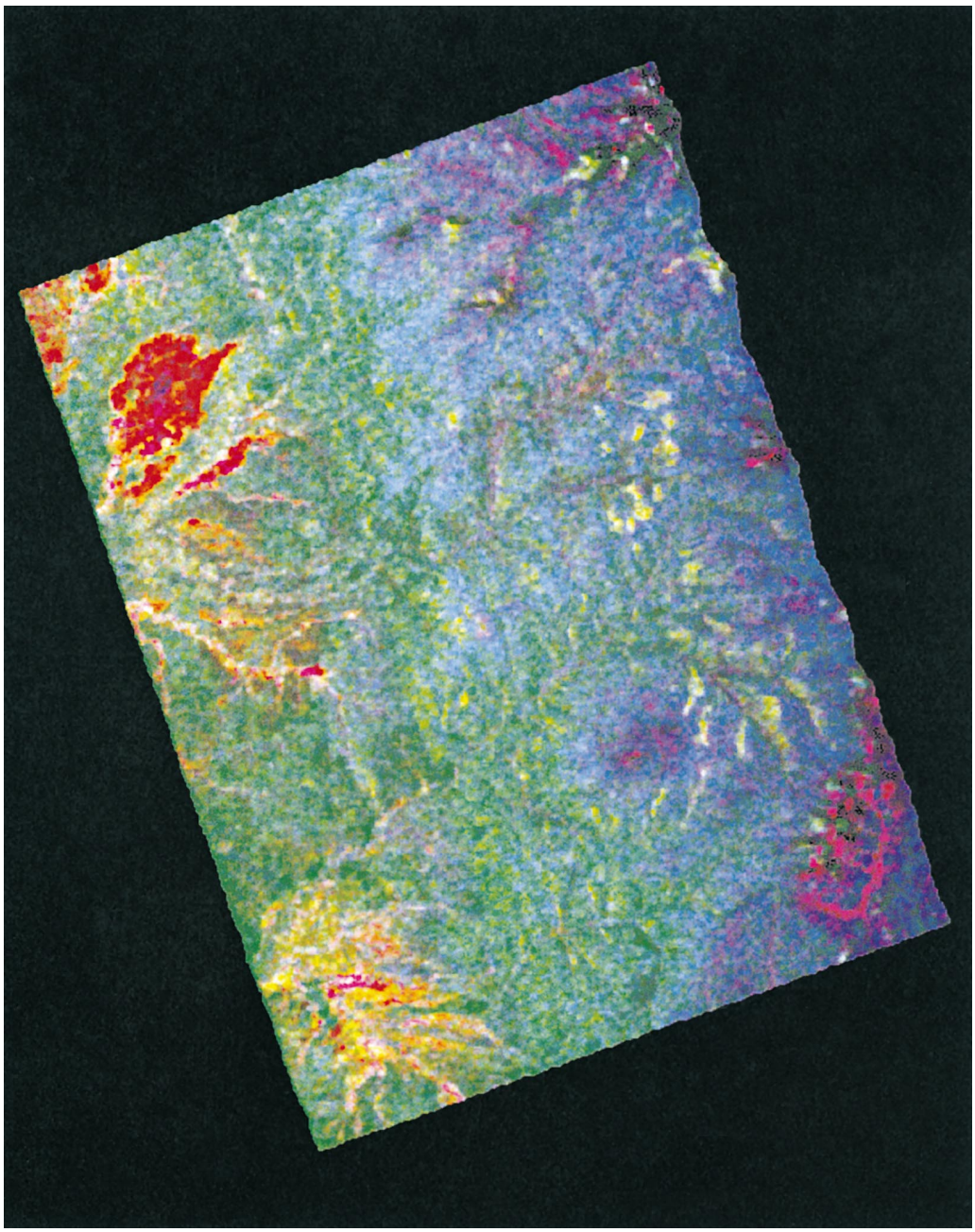

Figure 5. Composite image produced from first three principal components of SIR-C ratio images.

Classification with Ancillary Data

So far, the results indicate that a DEM is useful for radiometric correction, but that SAR channel ratios can be used to improve classification accuracy. However, topographic information can also be used to modify a classification based on knowledge of forest ecology. A straightforward way to do this is to use the known elevational limits of growth for forest species. For example, based on field surveys in the Sayani Mountains, aspen and birch do not grow above 760 m elevation and the highest elevation supporting tree growth (i.e., tree line) has been identified locally as 1,800 m. By applying some simple rules, the classification can be modified to reflect these limits. We did this by employing decision rules:

> If image class=YD and elevation is >760 m, then new image class=YC.
> If image class=OD and elevation is >760 m, then new image class=OC.

For cases of forest areas misclassified above tree line, if forests of any type are found, the pixels are relabeled as unknown since there is no logical class to replace it with:

> If image class=YD and elevation is >1,800 m, then new image class=unknown.

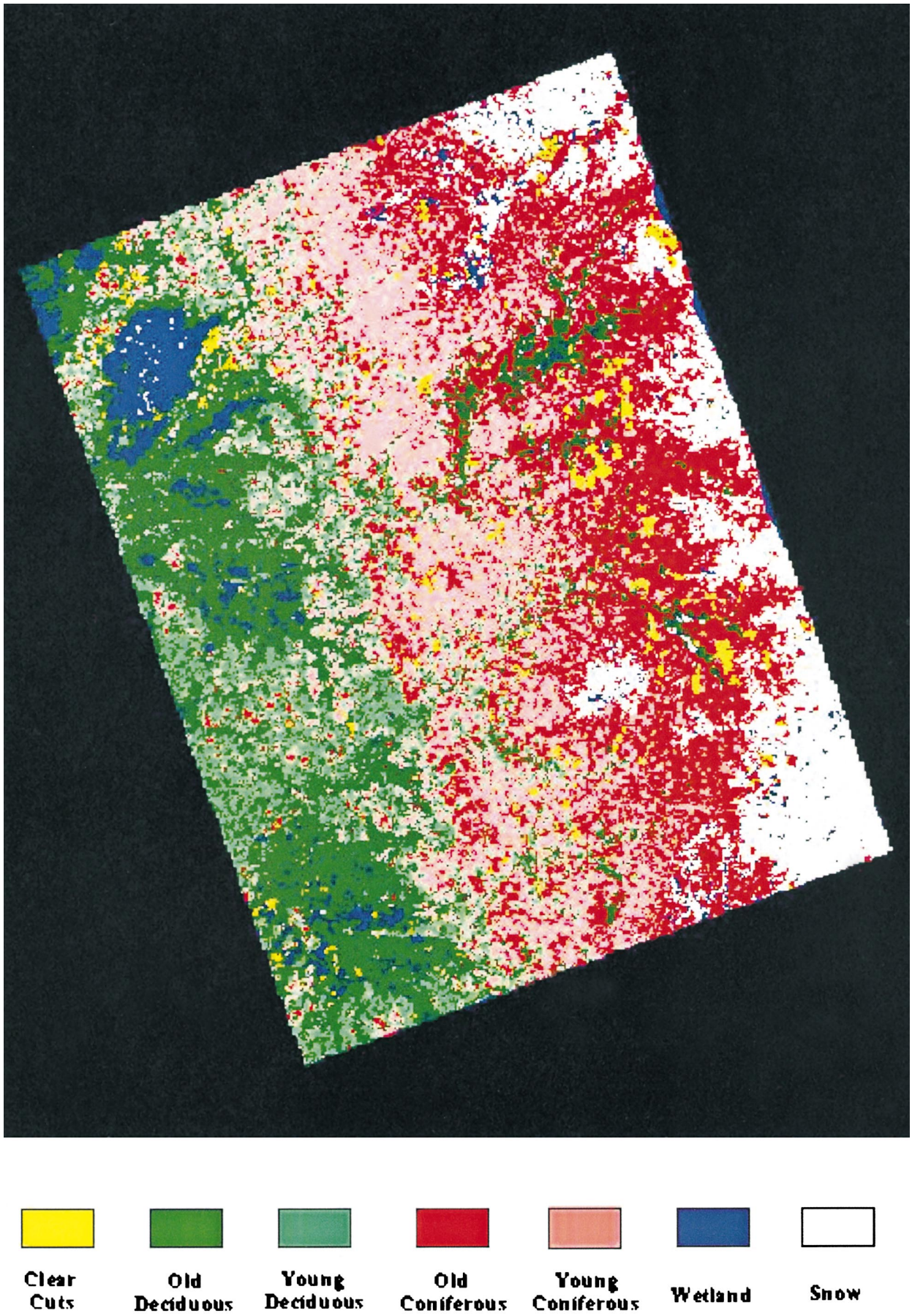

Figure 6. Final classification image produced with supervised maximum likelihood classifier with elevational rules imposed.

If image class=YC and elevation is >1,800 m, then new image class=unknown.
If image class=OD and elevation is >1,800 m, then new image class=unknown.
If image class=OC and elevation is >1,800 m, then new image class=unknown.

After imposing the elevational rules, young and old conifer test area accuracies increased by about 5%. Deciduous classes did not change appreciably. Combined conifer class results improved to 83%. However, the overall effect of imposing these rules on the classification was less than a 2% improvement in overall classification accuracy. Only 14 pixels were labeled as the unknown class in the classification process.

Table 10 summarizes the results for the training and test area analysis. Training data improved by about 5% for each new classification method attempted. Test area results improved by 25% using ratios and PC analysis over that of radiometric correction. Kappa values were also increased with largest improvement between using radiometrically corrected data and the PC of ratios method. Table 11 compares the percentages of the image occupied by each class for each classification method. Percent area covered by a class was mostly consistent between classifications using uncorrected and corrected SIR-C channels. Clear cuts decreased in classified area by 3.5%. There were larger decreases in young deciduous (∼6%) and old conifer (∼19%) percentages and an increase in snow percentage (∼9%) using the PC ratio methods as compared to using the SIR-C channels. The addition of the fifth and sixth PCs affected classified areas of clear cut, wetland, and young conifer and snow, but all less than 3%. The use of the elevational rules for the final classification decreased the classified area of old deciduous by about 5% and increased old conifer by a similar amount. Figures 5 and 6.

SUMMARY AND CONCLUSIONS

This work has demonstrated that effects of topography on forest classification in mountainous terrain are important and should be considered. We approached the problem in two ways: (1) radiometric correction using a DEM and (2) using band ratios to reduce the topography effect in the SAR data. PCA was used to reduce the total number of channels used in the classification. Radiometric correction using a simple algorithm substantially improved classification accuracy despite dependence on a rather poor quality DEM. PCA with 15-band ratios provided the best classification when selecting the first six PCs.

Old conifers in the study area are economically important and stands can be labeled as such even though only a few large trees are present. This will affect the performance of any remote sensing image classification as compared to these maps.

Topographic information can be used to reduce misclassifications when species elevation limits are known. Although not shown by the training and test area data analyses, the 5% change in the mapped areas of old deciduous and old conifer represent an improvement in the classification using elevation rules. A high-quality DEM such as that to be acquired by the Shuttle Topographic Mapping Mission in February 2000 is required to be able to use this information most effectively. Radiometric correction should also yield better results given a better DEM.

The latter point is an important one since the ratio technique requires multiple-channel SARs. The techniques and approaches here that utilize SIR-C data at this time cannot be broadly used since no operational satellite exists with multiple C- and L-band channels. There are plans to launch C-band multichannel SARs by Canada (Radarsat-2) and Europe (Envisat ASAR) and multichannel L-band (ALOS) by Japan in the next few years. While these data will be useful, there will still be difficulties due to the fact the data must be registered to use with satellite platforms with different imaging geometry. Overall the techniques presented and tested here hold promise for future forest mapping in mountainous terrain.

The study was partially supported by HASA HQ Office of Earth Science NASA grant NAG-5-3548 and RTOP 662-92.

REFERENCES

Colby, J. D. (1991), Topographic normalization in rugged terrain. *Photogramm. Eng. Remote Sens.* 57:531–537.

Colby, J. D., and Keating, P. L. (1998), Land cover classification using Landsat TM imagery in the tropical highlands: the influence of anisotropic reflectance. *Int. J. Remote Sens.* 19: 1479–1500.

Dobson, M. C., Pierce, L. E., and Ulaby, F. T. (1996), Knowledge-based land cover classification using ERS-1/JERS-1 SAR composites. *IEEE Trans. Geosci. Remote Sens.* 34(1):83–99.

Durden, S. L., Klein, J. D., and Zebker, H. (1991), Polarimetric radar measurements of a forested area near Mt. Shasta. *IEEE Trans. Geosci. Remote Sens.* 29(3):444–450.

Ekstrand, S. (1996), Landsat TM-based forest damage assessment: Correction for topographic effects. *Photogramm. Eng. Remote Sens.* 62:151–161.

Franklin, S. E. (1991), Image transformations in mountainous terrain and the relationship to surface patterns. *Comput. Geosci.* 17:1137–1149.

Goering, D. J., Chen, H., Hinzman, L. D., and Kane, D. L. (1995), Removal of terrain effects from SAR satellite imagery of Arctic tundra. *IEEE Trans. Geosci. Remote Sens.* 33(1): 185–194.

Goyal, S. K., Seyfried, M. S., and O'Neill, P. E. (1998), Effect of digital elevation model resolution on topographic correction of airborne SAR. *Int. J. Remote Sens.* 19(16):3075–3096.

Gu, D., Gillespie, A. R., Adams, J. B., and Weeks, R. (1999), A statistical approach for topographic correction of satellite images by using spatial context information. *IEEE Trans. Geosci. Remote Sens.* 37(1):236–245.

Kellndorfer, J., Pierce, L. E., Dobson, M. C., and Ulaby, F. T. (1998), Toward consistent regional-to-global-scale vegetation characterization using orbital SAR systems. *IEEE Trans. Geosci. Remote Sens.* 36(5):1396–1411.

Kharuk, V. I., Burenina, T. A., Onuchin, A. A., Fedotova, E. V., and Ranson, K. J. (1999), *Estimation of Snow Water Content by Microwave Sounding in the Forests of West Sayani,* Geografia I Prirodnie Resursi' (The Geography and Natural Resources), No. 4 (in Russian).

Leberl, F. W. (1990), *Radagrammetric Image Processing,* Artech House, Norwood, MA.

Paris, J., and Woodruff, R. (1991), Results from four years of field research with a C-band (6-cm) field microwave scatterometer in cultural- and natural-vegetation sites, IGARSS'91, pp. 2255–2256.

PCI, Inc. (1998), *PCIWorks User Manual,* Version 6.3, EASI/PACE, 50 West Wilmot Street, Richmond Hill, Ontario, Canada.

Pierce, L. E., Bergen, K. M., Dobson, M. C., and Ulaby, F. T. (1998), Multitemporal land-cover classification using SIR-C/X-SAR imagery. *Remote Sens. Environ.* 64(1):20–33.

Ranson, K. J., Saatchi, S., and Sun, G. (1995), Boreal forest ecosystem characterization with SIR-C/X-SAR. *IEEE Trans. Geosci. Remote Sens.* 33(4):867–876, July.

Ranson, K. J., and Sun, G. (1994), Mapping of boreal forest biomass from spaceborn synthetic aperture radar. *J. Geophys. Res.* 102(D24):29,599–29,610.

Ranson, K. J., and Sun, G. (1997a), Mapping of boreal forest biomass from spaceborn synthetic aperture radar. *J. Geophys. Res.* 102(D24):29,599–29,610.

Ranson, K. J., and Sun, G. (1997b), An evaluation of AIRSAR and SIR-C/X-SAR images for mapping Northern forest attributes in Main, USA. *Remote Sens. Environ.* 59:203–222.

Rignot, E. J. M., Williams, C. L., Way, J., and Viereck, L. A. (1994), Mapping forest types in Alaskan boreal forests using SAR imagery. *IEEE Trans. Geosci. Remote Sens.* 32(5): 1051–1059.

Saatchi, S., and Rignot, E. (1997), Classification of boreal cover types using SAR images. *Remote Sens. Environ.* 60:270–281.

Shi, J. C., and Dozier, J. (1997), Mapping seasonal snow with SIR-C/X-SAR in mountainous areas. *Remote Sens. Environ.* 59(2):294–307.

Smith, J. A, Lin, T. L., and Ranson, K. J. (1980), The Lambertian assumption and Landsat data. *Photogramm. Eng. Remote Sens.* 46:1183–1189.

Stofan, E. R., Evans, D. L., Schmullius, C., Holt, B., Plaut, J. J., van Zyl, J., Wall, S. D., and Way, J. (1995), Overview of results of Spaceborne Imaging Radar-C, X-band Synthetic Aperture Radar (SIR-C/X-SAR). *IEEE Trans. Geosci. Remote Sens.* 33 (4):817–828.

Sun, G., Simonett, D. S., and Strahler, A. H. (1991), A radar backscatter model for discontinuous coniferous forests. *IEEE Trans. Geosci. Remote Sens.* GE-29(4):639–650.

Ulaby, F. T., Moore, R. K., and Fung, A. K. (1986), *Microwave Rremote Sensing—Active and Passive,* Vol. III, Artech House, Inc., Dedham, MA.

Wever, T., and Bodechtel, J. (1998), Different processing levels of SIR-C/X-SAR radar data for the correction of relief induced distortions in mountainous areas. *Int. J. Remote Sens.* 19(2): 349–357.

Wu, S. T., and Sader, S. A. (1987), Multipolarization SAR data for surface feature delineation and forest vegetation characterization. *IEEE Trans. Geosci. Remote Sens.* 25: 67–76.